Solar activity and lunar precessions influence extreme sea-level variability in the U.S. Atlantic and Gulf of Mexico coasts

Arnoldo Valle-Levinson[a] and Jonathan B. Martin[b]

[a]*Department of Civil and Coastal Engineering, University of Florida, Gainesville, FL 32611 USA*

arnoldo@ufl.edu

[b]*Department of Geological Sciences, University of Florida, Gainesville, FL 32611 USA*

jbmartin@ufl.edu

Key Points:

Variations in detrended sea-level records display coherency between the Gulf of Mexico and the U.S. Atlantic seaboard.

An index representing variations in detrended sea-level records captures the timing of exacerbated coastal flooding events observed in the eastern U.S.

Periodicities related to the combined influence of solar activity and lunar precessions (*nodal & apsidal* or *perigean*) reproduce most variations of detrended sea-level in the eastern U.S.

The observed link between solar activity, lunar precessions, and sea level enables projections of the timing of anomalously high sea level for the rest of the 21st century.

Keywords: sea-level variations; solar activity; lunar precessions; eastern US; coastal flooding

Abstract

Inter-annual sea-level variations of up to 20 mm are superimposed upon the global average sea-level rise (~3 mm/yr) from human-caused global warming. These variations affect the degree of coastal flooding, and related damage, during the highest annual tides. Along the Atlantic coast of the United States, such inter-annual sea-level variations have been attributed to several atmospheric and oceanographic processes. In the present analysis, detrended tide gauge data isolate inter-annual interannual variations that can be reconstructed using Fourier analysis of a limited number of coefficients based on frequencies of lunar orbit (*nodal* and *apsidal* precessions) combined with *solar activity*. Although a causal relationship between such forcings and extreme sea levels remains elusive, the reconstructions may provide an effective method for projections of occurrence of extreme sea levels. Two reconstructions project that anomalously high sea levels may occur in the late 2020s, mid 2050s, early 2060s, early 2070s and late 2090s.

Introduction

A period of accelerated sea-level rise (SLR) over several years appeared along the southeast United States coast after 2011, with rates of SLR of upwards of 20 mm/year (~1 inch/year; Park and Sweet, 2015; Wdowinski et al., 2016; Valle-Levinson et al., 2017). This acceleration in SLR developed after several decades of multi-year accelerations in the rate of SLR as well as a notable spike in sea level from 2009-2010 north of Cape Hatteras, causing the region to be identified as a 'hot spot' of SLR (Boon, 2012; Ezer and Corlett, 2012; Sallenger et al., 2012). However, the discovery that similar multi-year accelerations had occurred in the southeastern United States (south of Cape Hatteras) in the late 1940s, in the early 1970s, and in the past decade indicates that such events are not confined to a single region and in fact occur simultaneously around the east coast of North America (Valle-Levinson et al., 2017; Domingues et al., 2018; Ezer, 2019). Consequently, these inter-annual variations in sea level are more appropriately referred to as "hot moments" of sea level rise.

Along the Atlantic seaboard of the United States, inter-annual variations in the rates of SLR in the last 100 years have been attributed to a number of processes, several of which may be interrelated. The timing of SLR accelerations has been ascribed to variations in nearshore wind forcing (Woodworth et al., 2014), to wind-driven Sverdrup transport in the subtropical gyre (Xie and Carton, 2004; Thompson and Mitchum 2014), or to the cumulative effects of ENSO that affect wind-driven transport in the Atlantic basin (Valle-Levinson et al., 2017). The latitudinal position of SLR accelerations, to the north or south of Cape Hatteras, has been attributed to warming of the Florida Current (Domingues et al., 2018) or to the NAO (Marshall et al., 2001; McCarthy et al., 2015). Other explanations for sea-level variability in the eastern seaboard of the United States have centered on the influence of longshore wind forcing (Piecuch et al., 2016); weakening of the Gulf Stream associated with decreased Atlantic Meridional Overturning

65 Circulation (AMOC, Ezer et al., 2013; Goddard et al.,2015; Ezer, 2015); the inverse barometer
66 effect (Piecuch and Ponte, 2015); a suite of ocean-atmosphere indices (Kopp, 2013); Rossby
67 wave modulation (Calafat et al., 2018); and ENSO events (Sweet et al., 2019). While it is clear
68 that several factors may affect sea-level variability and hence the timing of extreme coastal
69 flooding events, none of these studies has evaluated potential effects stemming from
70 astronomical forcing such as variations in lunar gravitational attraction and solar radiation nor
71 have they discerned a means of predicting when extreme coastal flooding by tides will occur in
72 the future. Astronomical effects could provide a master control over other Earth surface
73 processes that drive extreme sea level events (winds, tides, etc.) and if so, because they are
74 predictable, may provide a means to project when extreme events would occur.

75 The objective of this study is to explore the relation between sea-level variability in the eastern
76 U.S. and factors such as variations in lunar orbit and solar activity. Outside the eastern seaboard
77 of the United States, sea-level variability and the susceptibility of coastal regions to flooding by
78 tides have been linked to influences of lunar precessions at periodicities of 18.61 and 8.85 y and
79 their first subharmonics of 9.305 and 4.425 y (Eliot, 2010; Haigh et al., 2011; Peng et a., 2019).
80 Both lunar precessions (18.61, and 8.85 y, see *Supplementary Material* for a description) and
81 solar activity (10-11.5 y) have been described in dendrochronological records (Douglass, 1919;
82 1928; 1936), relating to ENSO history and the Pacific Decadal Oscillation (PDO) in the 20th
83 century (Yasuda, 2009; Berger, 2011). Furthermore, solar activity seems to be correlated with
84 increased appearance of storm surges in the northern Adriatic Sea (Barriopedro et al, 2010;
85 Zanchettin et al., 2009) and other European sites (Martinez-Ascencio et al., 2016). Elevated solar
86 activity corresponds to higher mean sea level in autumn and winter compared to periods with
87 low solar activity.

Several relevant questions arise from the findings outlined above. In particular, are inter-annual sea-level variations in the eastern U.S. connected to the influence of lunar precession and solar activity? Though much of the previous work on inter-annual sea level variations has focused on the Atlantic seaboard of the U.S., are there similar patterns of sea-level variability in the Gulf of Mexico? Might behavior in one region be able to predict future sea-level changes in another?

Methods

Decades-long tidal records allow exploration of the relationship between frequency of lunar precessions, outlined above, and solar activity with inter-annual sea level variations in the Gulf of Mexico. Also explored are links in sea level variations between the Gulf of Mexico and the eastern United States (through their Empirical Orthogonal Function, EOF mode 1). Data were obtained from the National Oceanic and Atmospheric Administration through their website "tidesandcurrents.noaa.gov". Hourly and monthly mean data were compiled at 11 stations of the US portion of the Gulf of Mexico starting between 1900 and 1982, depending on the station, and ending November 2019 (Figs. 1 and S1). Data with similar lengths and continuity as those in the United States portion of the Gulf of Mexico are unavailable for the Mexican portion of the gulf. The analysis with hourly data yielded the same results as with monthly means. Following data compilation, the record-long linear trend of sea-level rise was removed from each station.

Subsequent to removing the linear trend, intra-annual variations were filtered with a Lanczos filter centered at 1 year. This procedure followed that applied to data on the eastern United States (Valle-Levinson et al., 2017). The one-year low-pass filtered time series were then used to generate, via Delaunay triangulation, a regular matrix describing inter-annual variability of water levels (e.g. (Valle-Levinson et al., 2017). The matrix was drawn as a Hovmöller or phase diagram (Fig. 1) to illustrate timing and location of pronounced changes in sea level.

111 The matrix of one-year low-pass filtered sea level ***S*** was then decomposed into Empirical
112 Orthogonal Functions (EOFs), which are obtained by solving the eigenvalue problem of the
113 covariance matrix of ***S***. This analysis determines the dominant spatial structures (eigenvectors)
114 and their temporal variability (coefficients or principal components) of dominant modes.
115 Analysis in this study concentrated exclusively on principal component 1 as it is analogous to the
116 variability in the eastern United States. Principal component 1 explained 82% of the inter-annual
117 variability in the U.S. portion of the Gulf of Mexico. The principal component 1 was compared
118 to that from the entire east coast of the United States and also to that obtained from stations south
119 of Cape Hatteras (southeastern United States). After smoothing Principal component 1 with a 5-
120 yr Lanczos filter, this index was hereafter referred to as GOMSO (Gulf of Mexico Sea-level
121 Oscillation). The GOMSO index was subject to Fourier analysis decomposition for possible
122 influence from lunar precessions and solar activity. Reconstruction of GOMSO, via Fourier
123 coefficients with periodicities close to lunar precessions and solar activity is justified in the
124 *Supplementary Material*. The fraction of the observed variance explained by the Fourier
125 reconstruction, R^2, was calculated with the following expression:

$$R^2 = \frac{\sum[\bar{y}_{observed} - y_{reconstructed}]^2}{\sum[\bar{y}_{observed} - y_{observed}]^2}$$

126 where $\bar{y}_{observed}$ is the mean of all observations (e.g., GOMSO index), and $y_{reconstructed}$ is the
127 signal reconstructed with Fourier coefficients.

128 **Results**

129 The Hovmöller or phase diagram of one-year low-pass filtered and detrended sea level in the
130 Gulf of Mexico (Fig. 1, lower panel) displays common features in comparison to that in the
131 southeastern U.S. (Fig. 1 upper panel, consistent with Valle-Levinson et al., 2017). Anomalously
132 high sea level appeared throughout all 11 gulf stations in the late 1940s, centered in 1948, in the

early 1970s, centered in 1972-1973, and after 2011, mirroring the variability in the southeast U.S. The highest water levels throughout both of these regions appeared in the late 1940s and after 2011. Within the Gulf of Mexico, increases occur first on the eastern edge, in Key West, and take nearly one year to propagate westward to Port Isabel at the western edge of the U.S. gulf.

The spatial distribution of Mode 1 of the Empirical Orthogonal Functions (EOFs) displays changes that are largest in Galveston and Sabine Pass (Fig. 2a); both stations are in Texas (Fig. S1). This spatial distribution of Mode 1, together with its temporal variability, explains 82% of the variance at all stations in the U.S. portion of the gulf. The three highest peaks in inter-annual sea-level variability revealed in the coefficients of Mode 1 (Fig. 2b) correspond to the timing of those illustrated in the Hovmöller diagram: late 1940's, early 1970's and post 2011. Mode 1 of the EOF analysis of sea level along the entire U.S. Atlantic seaboard (explaining 62% of the variance) and for the EOF of the southeastern U.S. stations, south of Cape Hatteras, (explaining 83% of the variance) also show the anomalous highs around 1948, early 1970s and after 2011 (Fig. 2c). Thus, similarities of Mode 1 between the gulf and Atlantic records indicate a coherency in sea-level variations between the two regions, consistent with previous observations (Thompson and Mitchum, 2014) and with Figure S2.

The smoothed version of Mode 1 variability in the Gulf of Mexico, or GOMSO, is a representation of natural oscillations in detrended sea level records. The GOMSO index shows that the highest sea level was achieved in late 2016, simultaneous with the greatest number of events that exceeded 0.8 m relative to mean sea level at Virginia Key near Miami, Florida. There were 13 of such events in 2015, 15 in 2016, 8 in 2017, 4 in 2018, and 7 in 2019. In 2019, most events that exceeded 0.8 m were associated with onshore winds >10 m/s. The water level of 2016 could have also been related to hurricane activity (Ezer et al., 2017; Todd et al., 2018).

157 The GOMSO index can be reconstructed via Fourier coefficients (see Supplementary Material).
158 Only 5 Fourier coefficients, out of 608 possible for this time series, are needed to represent
159 >82% of the variance in GOMSO (Fig. S3). Using 10 and 15 Fourier coefficients represents
160 >97% and >99% of the variance, respectively (Fig. S3). The harmonics derived from this Fourier
161 decomposition have frequencies that are close to those of lunar precessions, solar activity and
162 their interactions (Fig. S3b). The analysis has relatively coarse frequency resolution to resolve
163 such interactions exactly. Therefore, rather than use the derived Fourier frequencies, we evaluate
164 if harmonics related to lunar precessions, solar activity, and their interactions also reproduce the
165 GOMSO. We use these frequencies (green lines on Figure S3b) because they have physical
166 explanations, are predictable, and are known to affect sea level. As we show below, these
167 frequencies reproduce the GOMSO. Although astronomical forcing has effects on sea level
168 variations (Supplemental Material), we caution that our reproduction does not necessarily reflect
169 a causal relationship. Any such relationship would be complicated by effects of astronomical
170 forcing on atmospheric and oceanic processes such as winds, atmospheric pressure, currents, and
171 heat transport.

172 Lunar precession harmonics have corresponding periods of T_n = 18.61 y (*nodal* precession
173 period), T_{nh} = 9.305 y (first subharmonic of the *nodal* precession period), and T_a = 8.85 y
174 (*apsidal* precession period). Reconstruction of the GOMSO index with only these 3 precession
175 harmonics produced a signal in which a few peaks nearly coincided in timing with GOMSO's
176 peaks of the 1940s, 1970s and post 2011 (Fig. 3a). Such peaks had differing amplitudes and thus
177 the reconstruction explained only 7% of the variance of GOMSO, although the signals coincided
178 (near-zero lag) at frequencies > 0.1 cycles per year (black line Fig. S4). Reconstruction with
179 solar activity, or sunspots, with harmonics of T_{s1} = 11.5 y and T_{s2} = 10 y, also produced a signal
180 in which some of the peaks nearly coincided with GOMSO (Fig. 3b). Coincidence again had

limited correspondence with amplitude and thus explained 10% of the variance of GOMSO. The signal reproduced with solar activity alone (Fig. 3b) showed some relationship, but below a 95% confidence level, with GOMSO at periods around 10-11 y and near-zero lag (magenta line Fig. S4). In both cases of reproduction with lunar precessions and with solar activity, the poor goodness of fit hinders projections of future variability.

Reconstruction of GOMSO improves dramatically by combining lunar precessions, solar activity and interactions or modulations that involve 8 and 10 harmonics (Fig. 3c). In the eight harmonics case, three harmonics are given by the lunar precession periods (T_n, T_{nh}, and T_a), one is a solar activity period (T_{s1}), three more represent interactions or interferences (T_n & $T_a \rightarrow$ 16.87 y, T_{s1} & $T_a \rightarrow$ 38.4 y, and T_n & $T_{s1} \rightarrow$ 30.1 y), and the eighth harmonic is the average of T_n & T_a (13.73 y). This reconstruction explains 69% of the observed variance (Fig. 3c). Adding one solar activity harmonic (T_{s2}) plus its interaction (T_n & $T_{s2} \rightarrow$21.61 y), for a total of 10 harmonics, explains 88% of the observed variance (Fig. 3d). In this reconstruction with 10 harmonics, the lunar precessions contribute proportionally 0.08, the solar harmonics provide 0.12, and interactions between these processes contribute 0.80. It is evident that such interactions dominate sea-level variations and are likely responsible for 'hot moments' in water level. The relationship between GOMSO and reconstructions with 8 and 10 harmonics is statistically significant at all periodicities and with near-zero lag (red & blue lines in Fig. S4). Similar reconstructions with the 10 harmonics of Figure 3e to EOF mode 1 of sea-level variability in the Southeastern U.S. (Fig. S5a) and the entire Eastern U.S. (Fig. S5b) provide consistent results to those in the Gulf of Mexico.

Discussion

The combined influence of frequencies derived from lunar precessions and solar activity periodicities yields a record that coincides with observations of extreme sea levels (Fig. 3c, d).

The superposition of the observed sea-level variability with monotonically rising sea level may explain the increase in frequency of high-tide flooding events in the eastern U.S. For example, from 2000 to 2015, high-tide flooding frequencies increased by 75% on the northeast U.S. coast and by 125% along the southeast U.S. coast (Sweet et al., 2018). The squared coherency between GOMSO and EOF Mode1 for the southeastern U.S. (Fig. S2a) shows values that exceed the 95% confidence level (equivalent to a correlation coefficient R^2 of 0.78) at periods of near 3.5, 6 and greater than 10 y. A similar relationship exists between the Gulf of Mexico and the entire east coast of the United States (Fig. S2a). This coherence analysis further demonstrates the linkage between the gulf and the eastern seaboard for inter-annual oscillations of sea level. Phase lags between coasts (Fig. S2b) are lower than 20º, generally meaning a response time <1 year. Positive phase lags indicate that the Gulf of Mexico variations lag behind those on the east coast at those frequencies < 0.1 cpy (period of 10 years). For a frequency of 0.09 cpy (period of 11 y), for example, the ~10 º lag indicates a delay of 0.3 years. The similarity between Gulf of Mexico and east coast oscillations in sea level and the adequacy of the fits allow projections of sea level variations for the rest of the 21st century.

Two approaches are shown here to project anomalously high sea levels in the future. The first approach involves 8 harmonics (Fig. 3c) and yields a projection that remains between the values of the last century (Fig. 3f). The interactions among all 8 harmonics show that extreme high-tide flooding events, also known as sunny-day flooding, for the rest of this century have increased probability of occurring around 2028-29, 2052, 2064, 2072, and 2098. The second approach to project anomalously high sea levels in the rest of the 21st century involves 10 harmonics or periodicities (Fig. 3d). The projection with these 10 periodicities (Fig. 3f) indicates anomalously high sea levels to be expected around the same times as with the projection with 8 harmonics, plus a possible high in 2036. These projections may provide predictive capabilities for

exacerbated flooding during future storms or high tides that can be leveraged by coastal planners. Such predictive capabilities are essential for coastal planning as indicated by the relationship between hot moments of sea level variations and coastal flooding. As shown by GOMSO (Fig. 2b), detrended mean sea-levels have been declining since autumn 2016 and indeed, fewer events that surpassed a given threshold relative to mean sea levels occurred in 2017, 2018 and 2019 than 2016 in the southeastern U.S. and in the Gulf of Mexico (Sweet et al., 2018). These regions, however, were also affected by hurricanes *Irma* (2017), *Harvey* (2017), *Florence* (2018), and *Michael* (2018) that caused damaging floods from storm surge and in some cases, intense, prolonged rainfall in coastal regions after the period of anomalously high sea level had waned. Had those hurricanes occurred one or two years earlier, it is likely that flooding would have been worse. Having a method to evaluate periods of anomalously high sea level could allow predictions of timing for potential coastal flooding.

Although several factors contribute to inter-annual variability in detrended sea level observations, the variability associated in the Gulf of Mexico and along the Atlantic seaboard of the U.S. appears to broadly respond to the combined influence of lunar precessions and solar activity. Solar activity may be linked to the North Atlantic mean sea level pressure (Kelly, 1997), to ENSO (Emile-Geay et al., 2007) and NAO(Kodera, 2002; Thieblemont et al., 2015; Martinez-Ascencio et al., 2016) variability, which in turn have previously been linked to sea-level variability in this region (Valle-Levinson et al., 2017; Sweet et al., 2019). Both solar activity combined with lunar precessions have been related to PDO variability (Berger, 2011).

Conclusions

Atmospheric and ocean heating related to solar activity, plus gravitational attractions from variations in the moon's orbit, appear to superimpose to influence the timing and magnitude of extreme sea-level variability. Although astronomical forcing may not be the direct control on

extreme sea-level variability and instead influence many other global phenomena, it does have predictable periodicities and amplitudes that allow for projections of times when extreme sea levels might be expected. Future projections of extreme sea level will be critical in evaluating the potential for coastal inundation distributions, coastal erosion extent, transportation disruption, limits of saltwater intrusion, algal bloom incidence, among other phenomena at local, regional and global scales.

Data and code availability

All data used for this manuscript were obtained from and are available at NOAA's website: "tidesandcurrents.noaa.gov". The codes used to generate results may be obtained by contacting the corresponding author directly.

Acknowledgments.

This study was funded by NSF projects OCE-1325227 and OCE-1332718. Data for this study were obtained from NOAA's tide stations (tidesandcurrents.noaa.gov),

References

Barriopedro D., R. García-Herrera, P. Lionello, and C. Pino. A discussion of the links between solar variability and high-storm-surge events in Venice, J. Geophys. Res., 115, D13101, doi:10.1029/2009JD013114 (2010).

Berger, W.H. Discovery of the 5.7-year Douglass cycle: a pioneer's quest for solar cycles in tree-ring records. The Open Geography Journal, 4, 131-140 (2011).

Boon, J. D. Evidence of sea level acceleration at US and Canadian tide stations, Atlantic Coast, North America, *J. Coastal Res*., **28(6)**, 1437–1445, doi:10.2112/JCOASTRES-D-12-00102.1 (2012).

Calafat, F.M., T. Wahl, F. Lindsten, J. Williams, E. Frajka-Williams. Coherent modulation of the sea-level annual cycle in the United States by Atlantic Rossby waves, *Nature Comm*, **9**, 2571, DOI: 10.1038/s41467-018-04898-y (2018).

Domingues, R., Goni, G., Baringer, M., & Volkov, D. What caused the accelerated sea level changes along the U.S. East Coast during 2010–2015? Geophysical Research Letters, 45, 13,367–13,376. https://doi.org/10.1029/2018GL081183 (2018).

Douglass AE. Climatic cycles and tree-growth. Washington: Carnegie Institution. vol. I (1919).

Douglass AE. Climatic cycles and tree-growth. Washington: Carnegie Institution. vol. II (1928).

Douglass AE. Climatic cycles and tree-growth. Washington: Carnegie Institution. vol. III (1936).

Eliot, M. Influence of interannual tidal modulation on coastal flooding along the Western Australian coast, *J. Geophys. Res*., **115**, C11013, doi:10.1029/2010JC006306 (2010).

Emile-Geay, J., M. A. Cane, R. Seager, A. Kaplan, and P. Almasi. El Niño as a mediator of the solar influence on climate, Paleoceanography, 22, PA3210, doi:10.1029/2006PA001304 (2007).

289 Ezer, T. Regional differences in sea level rise between the Mid-Atlantic Bight and the South
290 Atlantic Bight: Is the Gulf Stream to blame? Earth's Future, 7(7), 771-783,
291 doi:10.1029/2019EF001174 (2019).
292 Ezer, T., L. P. Atkinson and R. Tuleya. Observations and operational model simulations reveal
293 the impact of Hurricane Matthew (2016) on the Gulf Stream and coastal sea level,
294 Dynamics of Atmospheres & Oceans, 80, 124-138. doi:10.1016/j.dynatmoce.2017.10.006
295 (2017).
296 Ezer, T. Detecting changes in the transport of the Gulf Stream and the Atlantic overturning
297 circulation from coastal sea level data: The extreme decline in 2009–2010 and estimated
298 variations for 1935–2012. *Global and Planetary Change* **129**, 23-36,
299 doi:http://dx.doi.org/10.1016/j.gloplacha.2015.03.002 (2015).
300 Ezer, T., Atkinson, L. P., Corlett, W. B. & Blanco, J. L. Gulf Stream's induced sea level rise and
301 variability along the US mid-Atlantic coast. *Journal of Geophysical Research: Oceans*
302 **118**, 685-697 (2013).
303 Ezer, T., and W. B. Corlett. Is sea level rise accelerating in the Chesapeake Bay? A
304 demonstration of a novel new approach for analyzing sea level data, *Geophys. Res. Lett*.,
305 **39**, L19605, doi:10.1029/2012GL053435 (2012).
306 Goddard, P. B., Yin, J., Griffies, S. M. & Zhang, S. An extreme event of sea-level rise along the
307 Northeast coast of North America in 2009–2010. *Nature communications* **6** (2015).
308 Haigh, I. D., M. Eliot, and C. Pattiaratchi. Global influences of the 18.61 year nodal cycle and
309 8.85 year cycle of lunar perigee on high tidal levels, *J. Geophys. Res*., **116**, C06025,
310 doi:10.1029/2010JC006645 (2011).
311 Kelly, P.M. Solar influence on North Atlantic mean sea level pressure, Nature, 269, 320-322
312 (1977).

313 Kodera, K. Solar cycle modulation of the North Atlantic Oscillation: Implication in the spatial
314 structure of the NAO, Geophys. Res. Lett., 29(8), 1218, doi:10.1029/2001GL014557
315 (2002).
316 Kopp, R. E. Does the mid-Atlantic United States sea level acceleration hot spot reflect ocean
317 dynamic variability? *Geophysical Research Letters* **40**, 3981-3985 (2013).
318 Marshall, J., Johnson, H. & Goodman, J. A study of the interaction of the North Atlantic
319 Oscillation with ocean circulation. *J. Clim*. **14**, 1399–1421 (2001).
320 Martinez-Asencio, A., M. N. Tsimplis, and F. M. Calafat. Decadal variability of European sea
321 level extremes in relation to the solar activity, Geophys. Res. Lett., 43, 11,744–11,750,
322 doi:10.1002/2016GL071355 (2016).
323 McCarthy, G. D., Haigh, I. D., Hirschi, J. J.-M., Grist, J. P. & Smeed, D. A. Ocean impact on
324 decadal Atlantic climate variability revealed by sea-level observations. *Nature* **521**, 508-
325 510 (2015).
326 Park, J. & Sweet, W. Accelerated sea level rise and Florida Current transport. *Ocean Science*
327 *Discussions* **12**, 551-572 (2015).
328 Peng, D., Hill, E. M., Meltzner, A. J., & Switzer, A. D. Tide gauge records show that the 18.61-
329 year nodal tidal cycle can change high water levels by up to 30 cm. Journal of
330 Geophysical Research: Oceans, 124, 736–749. https://doi.org/10.1029/2018JC014695
331 (2019).
332 Piecuch, C. G., S. Dangendorf, R. M. Ponte, and M. Marcos: Annual sea level changes on the
333 North American Northeast Coast: influence of local winds and barotropic motions, J.
334 Climate, 29, 13, 4801-4816 (2016).

335 Piecuch, C. G. & Ponte, R. M. Inverted barometer contributions to recent sea level changes along
336 the northeast coast of North America. *Geophysical Research Letters* **42**, 5918-5925
337 (2015).
338 Sallenger Jr, A. H., Doran, K. S. & Howd, P. A. Hotspot of accelerated sea-level rise on the
339 Atlantic coast of North America. *Nature Climate Change* **2**, 884-888 (2012).
340 Sweet, W., Dusek, G., Marcy, D., Carbin, G., Marra, J., 2018 State of U.S. High Tide Flooding
341 with a 2019 Outlook, NOAA Technical Report NOS CO-OPS 090, 23 pp (2019).
342 Sweet, W.V., Dusek, G., Obeysekera, J., Marra, J.J. Patterns and Projections of High Tide
343 Flooding Along the U.S. Coastline Using a Common Impact Threshold, NOAA Technical
344 Report NOS CO-OPS 086, 44 pp (2018).
345 Thiéblemont, R. K. Matthes, N.-E. Omrani, K. Kodera & F. Hansen. Solar forcing synchronizes
346 decadal North Atlantic climate variability, Nature Comm., 6, 8268 (2015).
347 Thompson, P. R. & Mitchum, G. T. Coherent sea level variability on the North Atlantic western
348 boundary. *Journal of Geophysical Research: Oceans* **119**, 5676-5689,
349 doi:10.1002/2014JC009999 (2014).
350 Todd R. E, T. G. Asher, J. Heiderich, J. M. Bane, R. A. Luettich. Transient response of the Gulf
351 Stream to multiple hurricanes in 2017. Geophys Res Lett 45. doi:10.1029/2018GL079180
352 (2018).
353 Valle-Levinson, A., A. Dutton, and J. B. Martin (2017), Spatial and temporal variability of sea
354 level rise hot spots over the eastern United States, *Geophys. Res. Lett.*, **44**,
355 doi:10.1002/2017GL073926 (2017).
356 Wdowinski, S, Bray R., Kirtman B.P., Wu Z. Increasing flooding hazard in coastal communities
357 due to rising sea level: Case study of Miami Beach, Florida. *Ocean & Coastal*
358 *Management*, **126**, 1-8 (2016).

359 Woodworth, P. L., Maqueda, M. Á. M., Roussenov, V. M., Williams, R. G. & Hughes, C. W.
360 Mean sea-level variability along the northeast American Atlantic coast and the roles of the
361 wind and the overturning circulation. *Journal of Geophysical Research: Oceans* **119**,
362 8916-8935 (2014).
363 Xie, S-P and Carton, J.A., Tropical Atlantic Variability: Patterns, Mechanisms, and Impacts, in
364 Earth Climate: The Ocean-Atmosphere Interaction, C. Wang, S.-P. Xie, and J. A. Carton
365 (eds.), Geophysical Monograph, AGU, Washington, D.C. (2004).
366 Yasuda, I. The 18.6-year period moon-tidal cycle in Pacific Decadal Oscillation reconstructed
367 from tree-rings in western North America. *Geophysical Research Letters*, 36, LO5605
368 (2009).
369 Zanchettin, D., A. Rubino, P. Traverso, and M. Tomasino. Teleconnections force interannual-to-
370 decadal tidal variability in the Lagoon of Venice (northern Adriatic), J. Geophys. Res.,
371 114, D07106, doi:10.1029/2008JD011485 (2009).

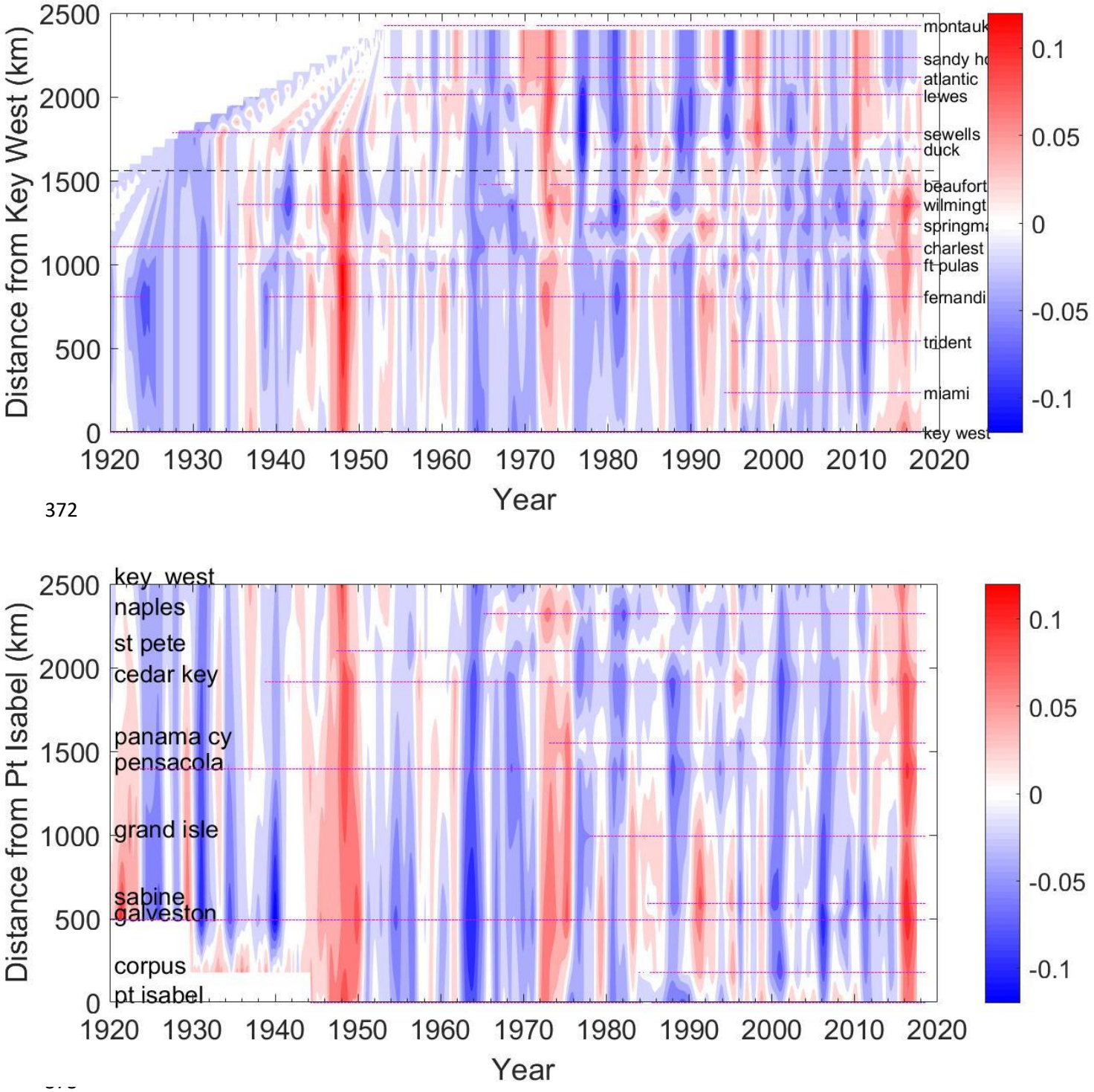

Figure 1. Hovmöller diagram of detrended, one-year low-pass filtered sea level (in meters) for the eastern United States (upper panel) and its portion of the Gulf of Mexico (lower panel). Magenta symbols indicate data coverage for each station (see Fig. S1 for station locations). Key West data coverage begins before 1920. Red bands indicate periods and locations of anomalously high sea levels (in the late 1940s, early 1970s and after 2011).

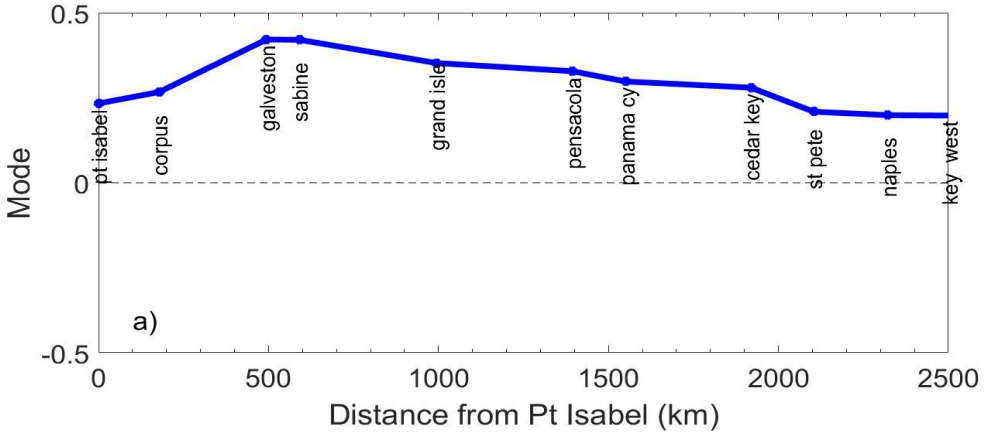

379

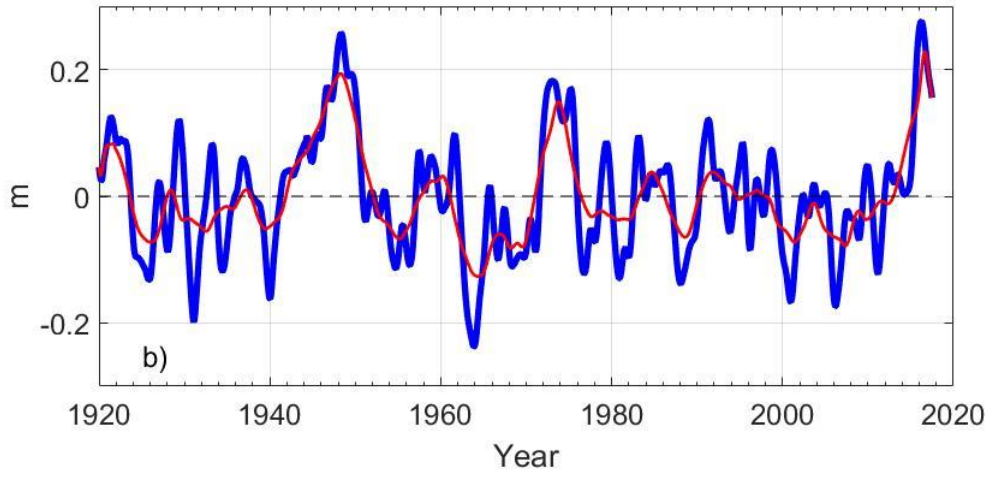

380

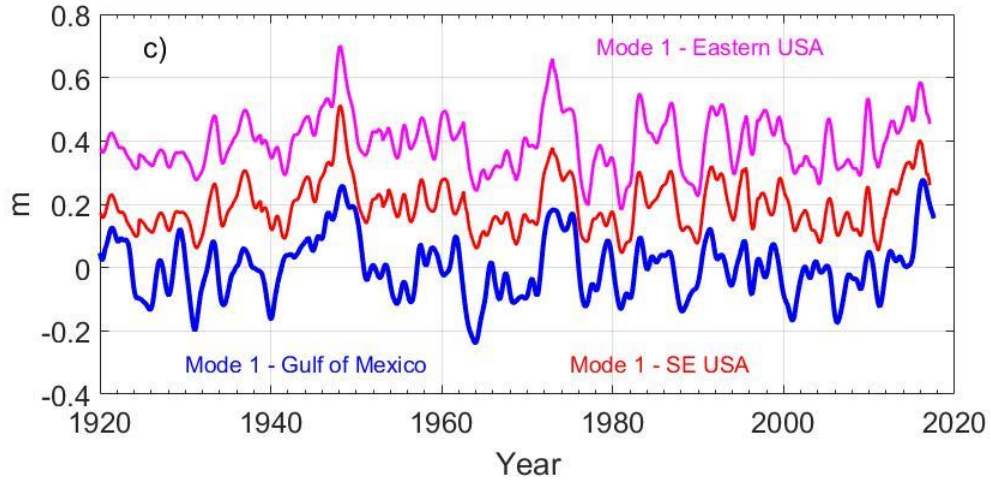

381

382 **Figure 2**. EOF results. a) Spatial structure of sea-level variability for Mode 1 in the Gulf of
383 Mexico. b) Temporal variability of Mode 1 coefficients in the Gulf of Mexico (Gulf of Mexico
384 Sea-level Oscillations – GOMSO, see text). These values should be scaled by (multiplied times)
385 the spatial structure given in Fig. 2a. Red line indicates 5-yr smoothing, representing an index of
386 sea level variations in the gulf. c) Mode 1 for the Gulf of Mexico (bottom), for the southeastern
387 (SE) coast only (middle), and for the entire east coast of the United States (top). Each record has
388 been offset by 0.2. In c) the 3 main pulses are seen in all records.

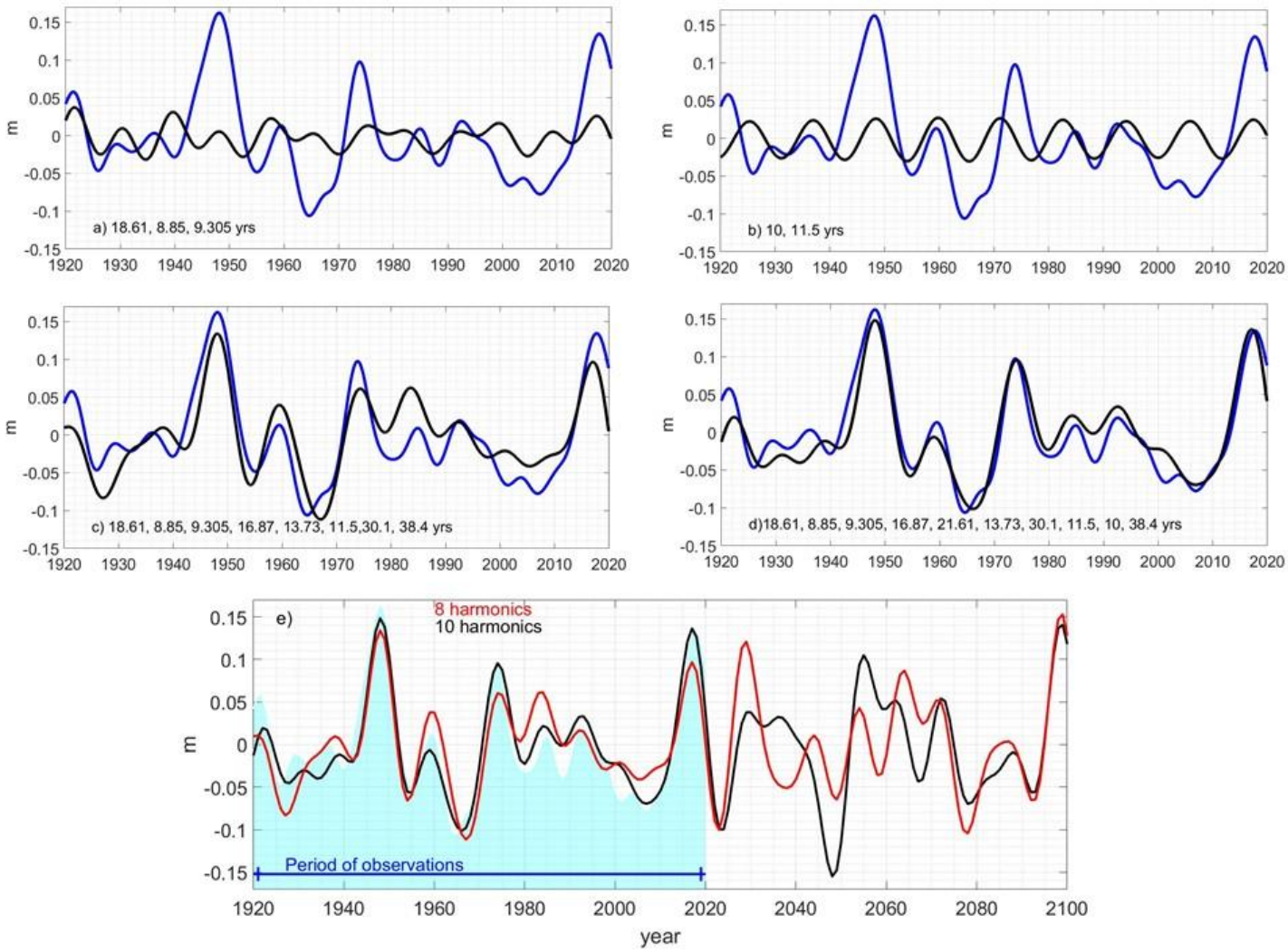

Figure 3. Reconstructions of GOMSO with different combinations of harmonics (a-d) and projection of sea-level variations for the rest of the 21st century. Harmonics used in the reconstructions are shown by green lines in Figure S2b. a) Reconstruction with harmonics only related to lunar precessions. b) Reconstruction only with solar activity harmonics. c) Reconstruction with 8 harmonics related to lunar precessions, one solar activity harmonic and modulations. d) Reconstruction with 10 harmonics describing lunar precessions, two solar harmonics and their interactions. e) Projections for the rest of the 21st century made with the 2 sets of harmonics shown in c), and d), plotted on top of the period of GOMSO observations (cyan shade). The red line is related to 8 harmonics in c) and the black line is associated with 10 harmonics in d). The two projections are consistent with each other.